The Crystal Structure and Surface Energy of $NaAlH_4$: A Comparison of DFT Methodologies

Terry J. Frankcombe*

Leiden Institute of Chemistry, Gorlaeus Laboratories, Leiden University, P.O. Box 9502, 2300 RA Leiden, The Netherlands

Ole Martin Løvvik

Center for Materials Science and Nanotechnology, University of Oslo, P.O. Box 1126 Blindern, N-0318 Oslo, Norway

Received: August 19, 2005; In Final Form: November 7, 2005

This paper presents a comparison of the bulk structure, cleavage energies, and local densities of states of solid $NaAlH_4$ calculated using several different density functional theory methodologies. Good agreement is obtained for the bulk crystal structure. Larger differences become apparent for the calculated surface energies and local densities of states. The (001) $NaAlH_4$ surface is clearly identified as the most stable surface, followed by the (112) and (101) surfaces, with the (100) surface being the least stable. We present an analysis of the local density of states of atoms in the exposed $NaAlH_4$ surface.

1. Introduction

Complex metal hydrides are leading candidates for lightweight and compact hydrogen storage materials, particularly for mobile applications.[1] Since the work of Bogdanović and Schwickardi demonstrating cyclable hydrogen storage in the presence of titanium-based additives,[2] much attention has been focused on the $NaAlH_4$ system and doping strategies. However, alternative light hydride phases with beneficial hydrogen storage properties are actively being sought.

Much of the exploration of potential hydrogen storage materials is being performed using computational investigations of known and hypothetical structures.[3−19] Typically, in these studies some flavor of density functional theory (DFT)[20−22] is used to calculate properties of the bulk solid or of the surface of the solid material. A wide range of DFT methodologies and implementations are currently in regular use for these predictive studies, with little attention being paid to any strengths or weaknesses of particular methods.

While in principle all accurate DFT calculations should give the same answer to the same question, all DFT implementations necessarily involve some level of approximation, such as the treatment of core regions, the representation of the electron density in a finitely storable manner, and the selection and implementation of the exchange-correlation functional. Of these three classes of approximation, the latter is the most easily controlled by the use of well-known, specified functionals. The representation of the electron density is also reasonably easily controlled and reproducible through the widespread use of plane wave basis sets. With plane wave basis sets, for any given unit-cell geometry, the basis set in which the electron density is expanded is exactly specified by a single energy cutoff. However, other forms of electron density representation, such as values on a regular grid or atom-centered basis functions, are regularly used in DFT implementations.

The first approximation mentioned above, that of the treatment of the core region of atoms, is possibly the most variable among different DFT implementations. Full-potential all-electron, frozen-core, and local or nonlocal pseudopotential calculations can be performed. Pseudopotentials or pseudopotential-like approaches can be implemented directly or embedded in the basis set in an augmented plane wave-like approach, of which there are several. Pseudopotentials are many and varied, and new ones can be readily generated by tweaking any one of a large number of parameters in the well-known families of pseudopotentials or by inventing a completely new pseudopotential function. All of this adds up to the treatment of core regions of atoms within the solid being modeled being difficult to specify precisely and, hence, being difficult to report in a manner that allows the results to be reproduced and thus trusted.

The difficulty of reporting reproducible calculations (even for "standard" methodologies such as "plane wave pseudopotential calculations using a GGA exchange-correlation functional") is not important if the results of relevant calculations are reasonably insensitive to implementation and methodology details. However, there have been few comparisons between different DFT methodologies published in the literature to test for sensitivity and to guide method selection. In this paper, we aim to perform direct comparisons between several different methodologies applied to the highly relevant $NaAlH_4$ structure in order to clarify how differences in methodology affect calculations on complex metal hydrides. We use available published data, as well as new results, as the basis for this comparison.

The first result to be presented is the calculated crystal structure of bulk $NaAlH_4$. This has been calculated by a number of studies already,[3−8] and our results in this part of the paper are compared to the available literature. The next part presents the calculated surface energy of selected low-index surfaces, followed by the projected densities of states on these surfaces. Despite the likely importance of the surface in the hydrogenation kinetics of $NaAlH_4$, very few studies have so far investigated

10.1021/jp054682u CCC: $33.50
Published on Web 12/09/2005

surface properties of the material, and this part of the paper is entirely dedicated to novel results.

2. DFT Methodologies

Three different implementations of DFT were used in this work, each differing in the methodology used. The main difference between the methods is the treatment of non-valence electrons.

ADF−BAND[23,24] is a periodic DFT program using atom-centered Slater-type and numerical atomic orbital basis functions. While all-electron calculations can be performed (representing, at the basis set limit, no approximate treatment of non-valence electrons), it is usual to apply the frozen-core approximation to non-valence atomic orbitals. With the frozen-core approximation, the electronic density calculated remains the all-electron density, but the Kohn−Sham orbitals are not optimized with respect to the basis functions contributing to the core orbitals. The atomic basis used in this work employs combined numerical and Slater-type atomic orbitals. The basis sets of Na and Al have 2s and 2p orbitals frozen, while two orbitals are added as polarization functions. The valence orbitals are described by the interpolation of two orbitals each.

DACAPO[25,26] is a periodic DFT program using the pseudopotential methodology.[27−29] In this approach, a pure plane wave basis set is used, but the nuclear potential is replaced by a pseudopotential designed to reproduce the behavior of the valence electrons outside a sphere centered on the nucleus which is defined by a particular cutoff radius. Only the valence electrons need then be modeled, and the required plane wave energy cutoff is vastly reduced from that needed to give a decent description of non-valence electrons. In this work, Vanderbilt ultrasoft pseudopotentials[30] have been used.

VASP[31,32] is a periodic DFT program using the projector augmented wave (PAW) method.[33−35] The PAW method is a generalization of the pseudopotential and augmented plane wave (APW) approaches, the latter of which was originally suggested by Slater.[36] In the PAW method, a plane wave basis set is used to express an auxiliary description of the density that is transformed into the full density by projectors that add the effect of local atom densities. In practice, this loosely corresponds to a frozen-core approximation with a plane wave expansion of the valence electrons.

These three codes represent a reasonable sampling of methodologies in current use for electronic structure calculations of periodic or crystalline systems. They also represent quite a range of "computational size" methods, loosely translating to different amounts of CPU time required to solve particular problems with each method. Generally, one would expect that the ordering of the CPU time to solve any particular electronic structure problem of medium size to translate to VASP and DACAPO being the fastest, with ADF−BAND taking significantly more CPU time for any particular calculation. While much faster methods do exist for large systems, these are not yet sufficiently accurate to perform realistic modeling of complex metal hydrides.[37]

We also discuss and compare with calculations performed by others using the codes WIEN2K and ABINIT. WIEN2K[38,39] is a periodic DFT program based on the APW+lo approach,[40,41] which uses plane waves with the effect of core electrons added in a muffin-tin-like manner. ABINIT[42] is a plane wave pseudopotential code, very similar in principle to DACAPO, mentioned above.

Throughout this work, the PW91 gradient-dependent exchange-correlation functional[43] was used, while results from the PBE functional[44,45] are also discussed. The convergence with respect to *k*-point density, integration accuracy, and basis set size has been thoroughly checked, and the overall convergence of the total energy is approximately 50 meV per conventional unit cell for ADF−BAND and DACAPO and 2 meV for VASP. For bulk $NaAlH_4$, convergence was attained with a $6 \times 6 \times 4$ Monkhorst−Pack[46] *k*-point grid and planewave and augmentation charge cutoffs of 780 and 400 eV, respectively, for the VASP calculations. For DACAPO, we used $4 \times 4 \times 4$ Monkhorst−Pack sampling and planewave and density cutoffs of 800 and 1600 eV, respectively. In all cases, the minimal unit cell (for example, the four formula unit crystallographic bulk $NaAlH_4$ unit cell) was used.

TABLE 1: Lattice Constants (Å) and Cell Volume (Å^3) for $NaAlH_4$ (space group $I4_1/a$)

	a	*c*	volume
this work, DACAPO	4.9412	11.1262	271.65
this work, VASP	5.0004	11.1141	277.90
Vajeeston et al.[a]	4.9965	11.0828	276.68
Ke and Tanaka[b]	4.979	11.103	275.25
Opalka and Anton[c]	5.008	11.123	278.97
Íñiguez et al.[d]	4.98	11.05	274.0
Peles et al.[e]	5.09	11.39	295.1
experiment[f]	4.9802	11.1482	276.50

[a] VASP, PBE, ref 3. [b] VASP, PW91, ref 4. [c] VASP, PW91, ref 5. [d] ABINIT, Troullier-Martins p.p. and PBE, ref 6. [e] Unspecified, Troullier-Martins p.p., ref 7. [f] Neutron diffraction, 8 K, ref 47.

TABLE 2: Atomic Coordinates of H for $NaAlH_4$ (space group $I4_1/a$, site 16f)

	x	*y*	*z*
this work, DACAPO	0.2404	0.3866	0.5452
this work, VASP	0.2350	0.3907	0.5442
Vajeeston et al.[a]	0.2199	0.3710	0.5639
Ke and Tanaka[b]	0.235	0.391	0.544
Íñiguez et al.[c]	0.2335	0.3918	0.5439
Peles et al.[d]	0.232	0.386	0.546
experiment[e]	0.2371	0.3867	0.5454

[a] VASP, PBE, ref 3. [b] VASP, PW91, ref 4. [c] ABINIT, Troullier-Martins p.p. and PBE, ref 6. [d] Unspecified, Troullier-Martins p.p., ref 7. [e] Neutron diffraction, 8 K, ref 47.

3. Bulk $NaAlH_4$

With the PW91 functional, the geometry of bulk $NaAlH_4$ was optimized by using VASP and DACAPO. ADF−BAND does not have the capability of calculating the forces on atomic nuclei, so no equivalent calculation can be performed with ADF−BAND without an inordinate expenditure of computational resources. While VASP allows optimization of the energy with respect to the atomic position and unit cell parameters simultaneously, DACAPO does not have this capacity without experimental extensions, meaning that atomic positions and unit cell parameters had to be relaxed sequentially until convergence was achieved. The residual minimization method with direct inversion in iterative subspace was used as an implementation of the quasi-Newton method for the relaxations using VASP. DACAPO used a steepest-descent method.

The resulting structural parameters are shown in Tables 1 and 2. A number of results taken from the literature are also shown in these tables for comparison. Vajeeston et al.[3] and Ke and Tanaka[4] used the PAW method of VASP with the PBE and PW91 functionals, respectively, to optimize the structure of $NaAlH_4$. Opalka and Anton[5] similarly used the PW91 functional with VASP but did not report coordinates for the hydrogen degrees of freedom. Íñiguez et al.[6] used the PBE

TABLE 3: Magnitude of Difference of Position in Coordinate Space of the Hydrogen atom in the 16f Site of $NaAlH_4$ (space group $I4_1/a$) for Six Available Geometries

		B	C	D	E	F	expt.[a]
this work, DACAPO	A	0.0069	0.0318	0.0071	0.0087	0.0084	0.0033
this work, VASP	B		0.0317	0.0004	0.0019	0.0059	0.0047
Vajeeston et al.[b]	C			0.0320	0.0319	0.0263	0.0297
Ke and Tanaka[c]	D				0.0017	0.0062	0.0050
Íñiguez et al.[d]	E					0.0063	0.0064
Peles et al.[e]	F						0.0052

[a] Neutron diffraction, 8 K, ref 47. [b] VASP, PBE, ref 3. [c] VASP, PW91, ref 4. [d] ABINIT, Troullier-Martins p.p. and PBE, ref 6. [e] Unspecified, Troullier-Martins p.p., ref 7.

functional with Troullier-Martins norm-conserving pseudopotentials with the ABINIT plane wave code, while Peles et al.[7] used a different set of Troullier-Martins pseudopotentials with an unspecified code and general gradient approximation (GGA) functional for the calculations that they report. The structural parameters determined experimentally for $NaAlD_4$ at 8 K by Hauback et al.[47] are shown for further comparison. The sodium and aluminum atoms are in sites of the $I4_1/a$ space group without degrees of freedom, being the 4*a* (0, $^1/_4$, $^1/_8$) site for sodium and the 4*b* (0, $^1/_4$, $^5/_8$) site for aluminum.

Not surprisingly, the eight geometries being considered here (the coordinates determined in this work by relaxation using DACAPO and VASP, the five previous relaxations taken from the literature, and the experimentally determined $NaAlD_4$ structure of Hauback et al.[47]) are very similar. The calculations performed with VASP that do not use pseudopotentials for core regions give cell volumes at 0 K varying by less than 1% from the experimental 8 K volume. The pseudopotential calculations perform worse in this regard, with the DACAPO calculations performed in this work (using ultrasoft pseudopotentials) underestimating the cell volume by almost 2% and the norm-conserving pseudopotential results published by Peles et al. overestimating the cell volume by almost 7%. The pseudopotential calculations of Íñiguez et al. do slightly better, with a 1% underestimation of the cell volume (and thus material density).

To quantify the small differences between the geometries, the differences in the relative cell coordinates of the hydrogen atom in each structure have been calculated. The magnitude of this difference (the length of the vector describing the displacement of the hydrogen atom when one moves from one structure to the other) is shown in Table 3. Clearly, a large magnitude in this table represents a large difference between the two structures (with a magnitude of 1.0 corresponding to traversal of the whole cell). The clear standout case in Table 3 is the structure calculated using VASP and the PBE functional reported by Vajeeston et al. The variation between the relative position of the hydrogen atom in this structure and the other structures (including the experimental structure) is an order of magnitude greater than that between all other pairs of structures. It should be noted, however, that this "worse" performance still represents reasonable agreement with the experimentally derived structure, with relative coordinates differing by around 0.01. There is no clear indication in the method used by Vajeeston et al. as to the origin of the discrepancy, as the PAW approach implemented in VASP gives H coordinates in good agreement with the others in this work and in the work of Ke and Tanaka, while the PBE functional used by Vajeeston et al. is successful in the calculations of Íñiguez et al. It is worth noting that the VASP/PW91 calculations of Ke and Tanaka agree precisely with the VASP/PW91 calculations performed in this work, to within the precision they quoted their hydrogen positions in. At that level of precision (three significant digits), a small difference in the calculated lattice parameters remains (Table 1).

Aguayo and Singh performed relaxation of the $NaAlH_4$ structure while maintaining the experimental lattice parameters.[8] In that work, they performed LAPW calculations with WIEN2K and determined hydrogen coordinates of (0.2364, 0.3906, 0.5451). This result is not reported in Tables 2 and 3 because of their use of the local density approximation (LDA) functional, a qualitatively different functional to the GGA functionals of the other calculations reported here. Despite this less sophisticated functional, these coordinates are of similar quality to those reported above with a relative coordinate distance from the experimental structure (Table 3) of 0.0040.

4. $NaAlH_4$ Surface Energies

Perhaps the most important issue in current hydride research is understanding the hydrogenation kinetics of $NaAlH_4$. To describe this by theoretical tools, it is crucial to know the properties of various surfaces of the hydride. A first step in this direction is to investigate the cleavage energy of some representative surfaces of the alanate, to tell what kind of surfaces are probably most common in pure $NaAlH_4$. This has already been done for $LiAlH_4$,[48] where it was found that the AlH_4 units should be kept intact and that the surfaces with the smallest number of broken Li−H bonds were the most stable ones.

We have investigated four different orientations of $NaAlH_4$ surfaces: (001), (100), (112), and (101). The latter surface may be constructed by cleaving in three different ways, with AlH_4, Na, or both AlH_4 and Na at the outer surface. We have thus calculated the cleavage energy of six different surfaces, shown in Figure 1. Note that the AlH_4-covered, Na-covered, and mixed surface (101) slabs are denoted here as (101) − Al, (101) − Na, and (101) − Na + Al, respectively, and that the (100) and (101) surfaces are identical to the (010) and (011) surfaces, respectively.

For the three-dimensional periodic calculations with VASP and DACAPO, the slabs that represent the various surfaces were constructed by inserting a vacuum layer with the relevant orientation into the appropriate unit cell. 10 Å of vacuum was found to be sufficient to reach converged cleavage energies. With ADF−BAND, it was possible to construct truly two-dimensional slabs because of the use of atom-centered basis sets rather than plane waves. Both methods result in two surfaces, which are generally identical, but different in the (101) − Na + Al case. In the former case, the cleavage energy is exactly the same as the surface energy. The latter case has been included in this study in order to describe as large a range of surfaces as possible without breaking the stoichiometry of the slab. The AlH_4 units were always kept intact when creating the slabs; test calculations have shown very high energy penalties for splitting these units.

As ADF−BAND does not have the capability to perform geometry optimizations, the cleavage energies were calculated with this program only at the bulk geometry optimized with VASP. For the cleavage energies calculated with VASP, both the experimental[47] and relaxed bulk geometries were used, along with fully and partially relaxed surfaces. By partially relaxed, we refer to the geometry where one surface layer of the slab was held fixed at the starting geometry to simulate continuation to the bulk, while the remainder was allowed to relax to the minimum-energy configuration. For the (101) − Na + Al slabs, the AlH_4 surface was kept fixed. From the DACAPO calculations, cleavage energies were calculated for the experimental

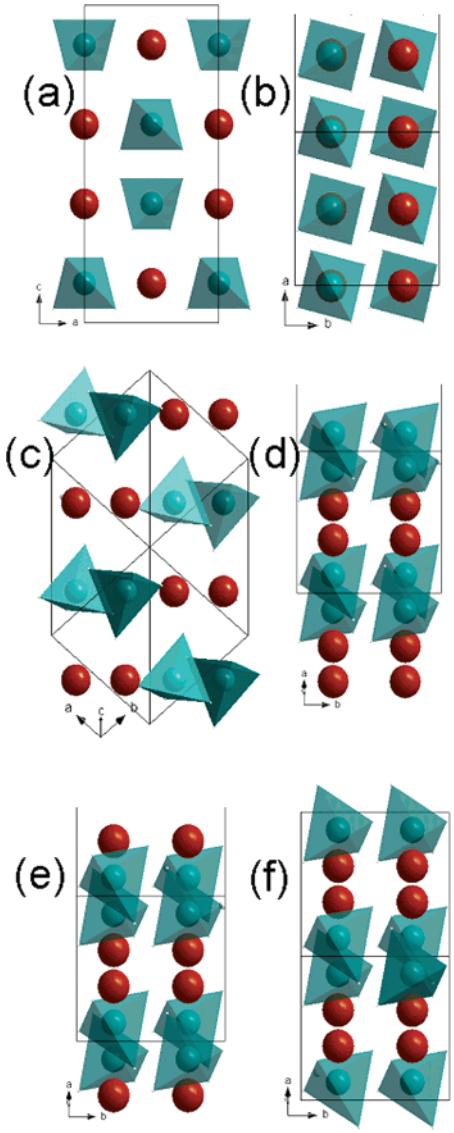

Figure 1. The six surfaces of $NaAlH_4$ that were studied: (a) (001), (b) (100), (c) (112), (d) (101) − Na + Al, (e) (101) − Na, (f) (101) − Al. Red balls and green tetrahedra denote Na atoms and AlH_4 units, respectively. The conventional unit cell is marked with thin lines. The surfaces are perpendicular to the page, oriented horizontally at the top and bottom of each slab.

bulk geometry and from fully relaxed surfaces only. The unit cell was kept constant, and only the atomic coordinates were relaxed.

The cleavage energy may be calculated in a number of ways, corresponding to how the surface energy may be calculated for metals.[49,50] The intuitive formula for calculating the surface energy is

$$E_{\text{surface}} = (E^N_{\text{slab}} - NE_{\text{bulk}})/A \qquad (1)$$

where E^N_{slab} is the energy for a slab of N "layers", A is the area of the slab surface per slab unit cell (including both surfaces), and E_{bulk} is the bulk energy per layer formula unit (that is, if each layer contains two material formula units per slab unit cell, E_{bulk} is the bulk energy per two formula units.) The problem for metals is the possibility of linear divergence of eq 1 because the bulk energy does not necessarily fit exactly to the change in the slab energy as layers are added.[51] Note that applying eq 1 to a series of slabs is actually a calculation of the cleavage energy. The surface energy is only equal to the cleavage energy if the surfaces on each side of the cleavage plane are equivalent (otherwise, the cleavage energy is the average of the two distinct surface energies).

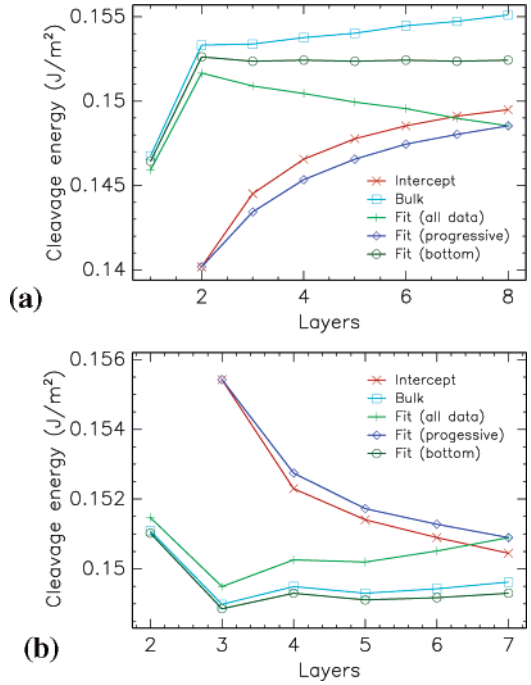

Figure 2. The convergence of the cleavage energy of the (001) surface calculated using various methods from energies calculated with VASP. See the text for a description of the different methods. (a) Results from slabs frozen at the experimental[47] bulk geometry. (b) Results from fully relaxed slabs.

A number of alternative ways of calculating the surface energy have been suggested.[49,50] In this work, we have explored several different methods, starting from the direct application of eq 1 using the calculated energy from a separate bulk calculation ("bulk") and interpreting the intercept of the best linear fit to the successive slab energies as $2E_{\text{surface}}$ ("intercept"). The slope of the linear fit to all slab energies was used as E_{bulk}, as advocated in ref 49 ["fit (all data)"], as well as several variations on this idea, including performing the fit for E_{bulk} to successively larger sets of slab energies and looking for convergence ["fit (progressive)"] and using the slope of the slab energies for the largest slabs (corresponding to adding four formula units or one crystallographic unit cell) as E_{bulk} ["fit (bottom)"]. In all cases, the number of layers was defined as the number of $NaAlH_4$ formula units in the slab unit cell. Note that in some cases this restricted the calculation of slab energies to, for example, slabs containing an even number of layers.

Examples of the convergence of the various methods are shown in Figure 2 for the (001) surface with energies calculated using VASP. While using the intercept of the best fit line as $2E_{\text{surface}}$ appears to be converging with increasing slab thickness, the rate of convergence is too low to be useful. Fitting to the slab energies as the slab thickness increases shows a very similar convergence behavior. This indicates that the idea of using the slope of the whole data set as E_{bulk} (advocated in ref 49) is misguided. Not only does using this fitting procedure [fit (all data)] produce unstable surface energies from successive slab thicknesses, the behavior of the progressive fit [which must necessarily meet fit (all data) at the largest slab] indicates that quite thick slabs would be required to demonstrate satisfactory convergence of the surface energy. Using the bulk energy from a separate calculation usually produces divergent surface energies (to a greater or lesser degree). Clearly, the most stable and

TABLE 4: Calculated Cleavage Energies in J/m^2 of the Six Different Surfaces Shown in Figure 1[a]

		ADF−BAND				VASP		DACAPO	
surface	broken bonds	LDA	BP	PW91	PBE	unrel.	rel.	unrel.	rel.
(001)	16.0	0.292	0.119	0.150	0.146	0.153	0.153	0.187	0.138
(100)	21.6	0.735	0.607	0.634	0.628	0.522	0.403	0.568	0.315
(112)	17.2	0.386	0.235	0.266	0.263	0.259	0.206	0.261	0.188
(101) − Al	19.7					0.310	0.274	0.362	(0.005)
(101) − Al + Na	26.3					0.283	0.231	0.640	(0.074)
(101) − Na	19.7					0.296	0.240	0.309	(0.157)

[a] The ADF−BAND energies are calculated within the local density approximation (LDA) and three different GGAs: BP,[52,53] PW91,[43] and PBE.[44] VASP and DACAPO calculations used the PW91 functional. The number of broken Na−H bonds (where the distance between Na and H is less than 3 Å) per nm^2 cleavage area is also shown for each surface. Relaxed DACAPO results (shown bracketed) are considered incorrect.

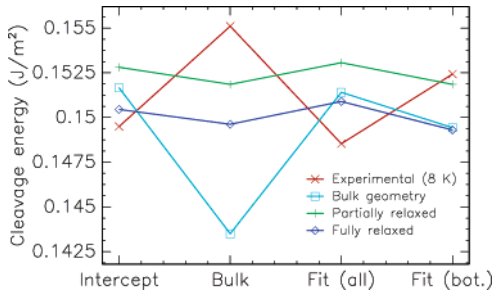

Figure 3. The variation in the calculated cleavage energy of the (001) surface with changes in the methodology (the treatment of the slab geometry and the extraction of cleavage energies from the slab energies). Slab energies were calculated with VASP. See the text for a description of the different methods.

efficient method for calculating the surface energies shown in Figure 2 is that labeled fit (bottom): using the slope of the largest slab energies for E_{bulk}. Such an approach effectively averages out the difference energy oscillations seen as non-equivalent layers are added.[48]

Figure 3 shows the cleavage energies calculated for the (001) surface from the energies calculated with VASP. Four cleavage energy calculation methods were selected [leaving out fit (progressive) from those shown in Figure 2], and data are shown for the 4 slab geometry classes used. Slabs up to 8 layers thick were considered. Each of the 16 combinations of geometry and cleavage energy derivation yields a different numerical value for the cleavage energy. Using the bulk energy in the determination of the cleavage energies yields the widest range of values, as expected, given the known linear divergence that arises with this approach. Contrary to expectation, Figure 3 indicates that the 3 other ways of calculating the cleavage energies shown give roughly the same spread of calculated cleavage energies. In particular, using the linear fit to the energies of only the thickest slabs to determine E_{bulk} does not give a more precise way of calculating the cleavage energies when the different ways of choosing the slab geometry are considered. This is despite the significantly greater stability of this method with respect to the slab thickness (Figure 2).

With the above results in mind, we have calculated the cleavage energies of the (001), (100), and (112) surfaces with ADF−BAND and of all six surfaces with VASP and DACAPO. Slabs up to eight layers thick were considered. The resulting cleavage energies are found in Table 4. For the (001), (100), and (112) surfaces, the slab energies were calculated using ADF−BAND with four different exchange-correlation functionals: the local density approximation (LDA), BP,[52,53] PW91,[43] and PBE.[44] In all cases, the LDA gave higher cleavage energies than the various GGAs (up to twice as high), which is consistent with the familiar overbinding of the LDA. The three GGAs gave cleavage energies that are quite similar, although the calculated cleavage energies were ordered consistently with the BP functional giving the lowest cleavage energies and the PW91 functional giving the highest. Nonetheless, the PW91 and PBE functionals gave very similar results.

The number of broken Na−H bonds per unit area of cleavage is shown for the various surfaces in Table 4 when we consider a Na−H bond to be present when the two nuclei are closer than around 3 Å. The cleavage energies shown in Table 4 correlate very well with this measure, with the (001) surface consistently exhibiting the lowest cleavage energies and (100) the highest. The (001) surface also exhibits the lowest change in the cleavage energy on relaxation of the slab: less than 1 mJ/m^2 for the energies calculated with VASP. The other surfaces have much more pronounced relaxation effects, giving the relatively large differences in cleavage energies in Table 4.

For the three (101) surfaces, the calculation of the cleavage energy with VASP and DACAPO for the unrelaxed geometry and with VASP for the relaxed geometry had few complications. On the other hand, relaxing the geometry with DACAPO resulted in unrealistic structures and surface energies. While energetically the (101) − Al surface was the most strongly affected, producing a very small surface energy, the relaxed geometry of the (101) − Al + Na slab was clearly altered from the structure of bulk $NaAlH_4$ and all the other structures considered in this work. The AlH_4 units rearranged into bridged trigonal bipyramidal structures with a surface hydrogen vacancy. We consider these relaxed (101) cleavage energies unreliable.

Like the other surfaces described above, the (101) cleavage energies derived from DACAPO calculations for the unrelaxed geometries were larger than those calculated with VASP. The DFT calculations performed with VASP and DACAPO predicted a completely different stability ordering. While the VASP calculations predicted that cleavage along a (101) plane will occur in such a way to leave two layers of sodium on one surface and none on the other [(101) − Al + Na], the DACAPO calculations predicted that this is in fact the least energetically favorable cleavage by a significant amount and that the easiest cleavage is between the sodium layers [(101) − Na]. The ordering derived from the unrelaxed DACAPO calculations is much more in accord with the ordering predicted by the notion that the cleavage energy correlates with the number of Na−H bonds broken in the cleavage.

Unlike the $NaAlH_4$ bulk structural properties discussed above, there are clear differences between the cleavage energies calculated from the three different DFT implementations. Restricting ourselves to the PW91 ADF−BAND results and the unrelaxed VASP and DACAPO results so as to compare like with like, differences of up to 22% are evident in the calculated clevage energies of the well-behaved (001), (100), and (112) surfaces. For the mixed (101) − Al + Na surface, the cleavage energy from the DACAPO slab energies is more than double that from the VASP energies. Yet, at the same time, some of the results are remarkably consistent, such as those for the (112)

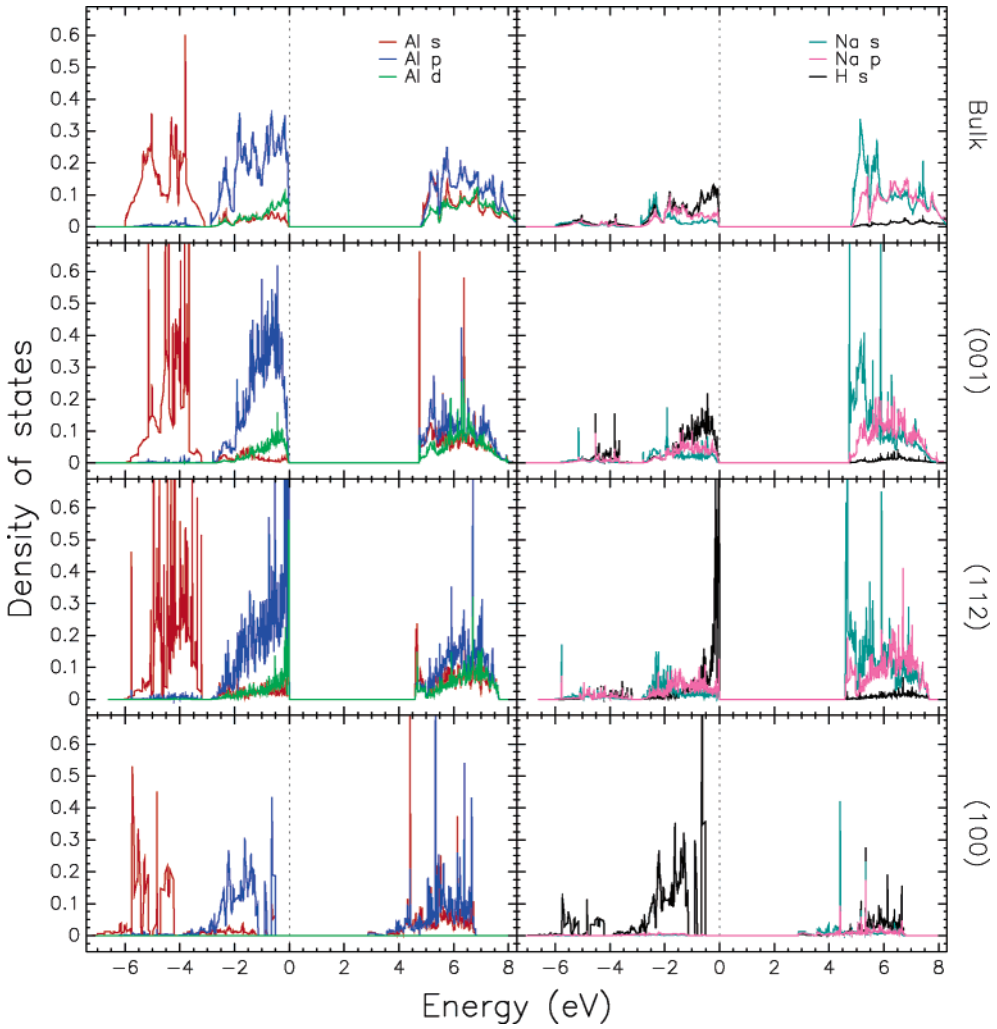

Figure 4. The local DOS projected onto atomic orbitals for bulk $NaAlH_4$ (top) and atoms in three surface structures (second, third, and bottom rows), calculated with VASP.

surface where all three codes agree to within 3%, close to the "slab energy to cleavage energy" uncertainty implied by Figure 3.

When the relaxed surfaces are considered, the differences become more consistent. After being consistently larger than the cleavage energies calculated using VASP for the unrelaxed surfaces, the cleavage energies calculated using DACAPO were found to be consistently smaller than those calculated with VASP on relaxation. This highlights the significantly larger relaxation effect in the energies calculated with DACAPO compared to those calculated with VASP, varying from an ~8% greater reduction in the cleavage energy for the (112) surface to the extreme effects shown for the (101) surfaces.

5. Surface Atom Densities of States

The local (or "projected") density of states (DOS) is commonly used as a qualitative indicator of bonding within a structure.[54] We have calculated local DOSs centered on atoms in the bulk $NaAlH_4$ structure and for the surface atoms in the (001), (100), and (112) surfaces of eight formula unit slabs. The covalent radii of the elements were used as the cutoff radii for the DOS projection.

A detailed view of the projected DOS, calculated with VASP, is shown in Figure 4. Here, the calculated DOSs have been projected on the orbital wave functions of three representative surface atoms and compared to the bulk results. The three atoms are the uppermost of their species at the particular surface, which means that they all are involved in the bond breaking at the surface, either directly (Na and H) or indirectly (Al via its nearest-neighbor hydrogen).

The changes in the DOS when creating a surface are closely connected to the breaking of Na−H bonds. First of all, it is evident that the DOS projected on a Na surface atom is considerably reduced below the Fermi level compared to the bulk. Correspondingly, the ADF−BAND-calculated Hirshfeld charges show that the integrated electron population around Na has decreased after creating the surface: from 10.73 electrons in the bulk to 10.66, 10.64, and 10.60 electrons at the (001), (112), and (100) surfaces, respectively. The effect thus follows the trend in the stability of the surfaces, but is nevertheless somewhat surprising. Intuitively, we could expect that a broken Na−H bond would leave the Na ion with more electrons, not less. But at the same time, the neighboring AlH_4 unit has experienced a bond loss, which must be compensated. It is well-known that this unit is very stable with regard to the temperature[55] and to different chemical surroundings in the bulk.[56,57] Thus, we should expect that it will gain charge from neighboring atoms to compensate the loss of this bond. This is seen in the calculated Hirshfeld charges, where the surface AlH_4 unit has a higher electron density than in the bulk, exactly balancing the loss from Na (the surface is charge neutral in all cases). All the atoms in the unit have gained charge, but the hydrogen atoms

TABLE 5: Calculated Band Gaps for $NaAlH_4$ Bulk and Three Surfaces (eV)[a]

	DACAPO	VASP	ADF−BAND
bulk	4.3	4.8	4.3
(001)	4.5	4.7	4.1
(100)	3.2	3.3	
(112)	4.5	4.5	

[a] (100) band gap calculated without reference to the Fermi energy.

that have lost one or two bonds have gained the most. In the bulk, hydrogen atoms form ionic bonds with Na and mostly covalent bonds with Al,[7,8] but in the surface, this is slightly changed. The H atoms that lost the bonds are still ionic in nature, but now, the ionic bond is formed with the Al atom. The Al atom compensates the electron loss from this bond by pulling electrons from the other H atoms. In turn, they take electrons from the surroundings, keeping the remainder of the AlH_4 unit intact. The net effect is that the bond losses are overcompensated, and the Na atom is thus losing electrons compared to the bulk.

The same behavior can be seen when studying the DOS projected onto H. The most important interaction between Na and H in the bulk is seen in the peak between −3 and −2 eV. This peak disappears to a large extent at the (001) surface (where one bond is lost from the upper H atom) and totally at the (112) surface (where both the bonds are lost). There is instead a significant increase in the electron density just below the Fermi level, corresponding to the new ionic bond with Al.

The band gap of $NaAlH_4$ is almost 5 eV, in accord with previous studies.[3,4,8,57] This seems not to be the case, however, for the atoms at the (100) surface, where the band gap is close to 3 eV (Table 5). It also seems that most of the bands have moved down in energy by approximately 1 eV. We believe this to be due to molecular-like surface bands that exist in the band gap of the bulk electronic structure, giving rise to a shift in the calculated Fermi level by around 1 eV. If such a shift is removed, the DOSs of the atoms at the (100) look quite similar to those of the other surfaces, except for the states that are present in the band gap.

Examination of the local DOSs for the various $NaAlH_4$ structures from the three codes used in this study reveal some intriguing features. Some of these are demonstrated in Figure 5, which shows a selection of the local DOSs calculated in this work. Contributions from s, p, and d orbitals have been summed into the atom-centered local DOSs and the total DOS (as opposed to the orbital-resolved data shown in Figure 4). Note that smearing has been applied to the DACAPO results and not to the VASP or ADF−BAND results.

The local DOSs calculated by VASP and ADF−BAND generally agree well for occupied states of the bulk and (001) structures. ADF−BAND produced a significantly larger DOS for bulk H states than VASP, however. The calculations of

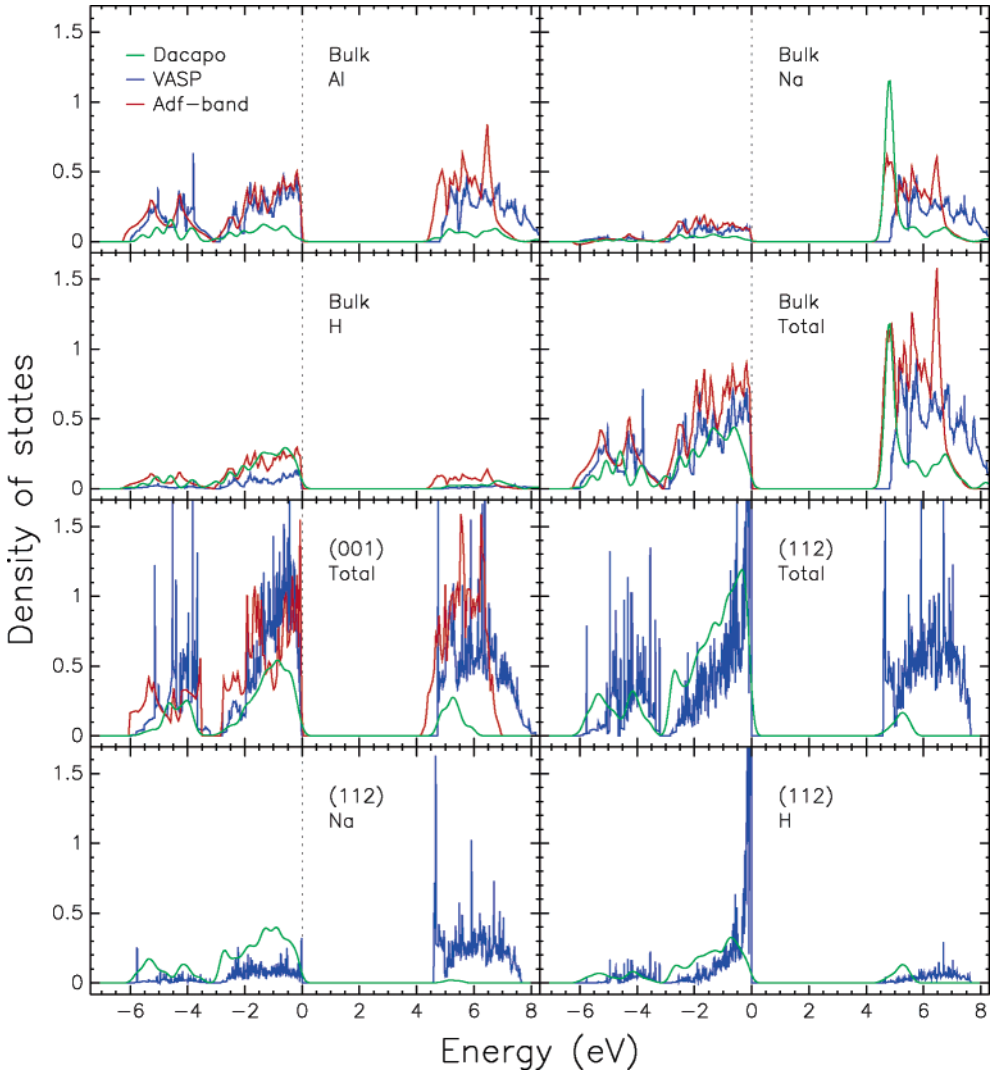

Figure 5. Selected local DOSs projected onto atomic centers for $NaAlH_4$, calculated with DACAPO, VASP, and ADF−BAND.

DACAPO produce quantitatively different DOSs, but the qualitative agreement is reasonable, with states partitioned into two groups lying in the −6.5 to −3 eV and −3 to 0 eV ranges. Yet, there are qualitative differences between the DACAPO results and those of VASP and ADF−BAND that are not reflected in Figure 5. For example, the low-energy states between −6.5 and −3 eV (primarily Al and H s states) are composed of roughly equal proportions of Al and H states for the DACAPO calculation, whereas VASP calculates this region to be primarily due to Al s states (Figure 4).

For the (100) surface (not shown in Figure 5), a similar level of agreement is seen between the VASP-calculated and DACAPO-calculated local DOSs as for the bulk case. For the (112) surface, the total DOSs agree quite well in the occupied region, considering the smearing applied in the DACAPO case (though a shift of the Fermi level would strengthen the agreement). However, the contributions to the total DOSs from Na and H states are completely different for the VASP and DACAPO calculations, with the former yielding negligible Na contribution and high H density of states below the Fermi level and the latter proportioning non-Al states roughly equally between Na and H. The vacuum states for the (112) surface seem mostly absent from the DACAPO results. The DOSs projected onto Al orbitals agree quite well between the codes below the Fermi level.

There is little agreement between the DOSs calculated by the three codes for vacuum states beyond general band gap agreement. The calculated band gaps for the various structures are shown in Table 5. The band gaps derived from the three sets of calculations differ significantly, with an irregular pattern of agreement between the codes. For the bulk structure, DACAPO and ADF−BAND agree, whereas VASP produced a band gap 0.5 eV larger. The (001) surface band gap is similarly predicted to be 0.6 eV larger by VASP than ADF−BAND, with DACAPO predicting an intermediate band gap. However, for the less stable (100) and (112) surfaces, for which ADF−BAND DOS calculations were not performed, the band gaps calculated with VASP and DACAPO agree well.

6. Conclusion

In this work, we have used VASP, DACAPO, and ADF−BAND to calculate bulk structures and surface properties of $NaAlH_4$. Of the surfaces considered (which included all "reasonable" low-index surfaces), the (001) surface was identified unambiguously as having the lowest cleavage energy to create the surface, and thus is the most stable. However, we have considered only the cleavage energy, so, though we consider this unlikely, we cannot exclude the possibility that one of the surfaces of our (101) − Al + Na slab could have a lower surface energy. Also, most certainly, the real material does not exhibit the pure, perfect surfaces considered in this idealized study, but rather, surfaces with impurities and defects. How this affects the relative stability of the various surfaces is clearly beyond the scope of the present study.

It is well-known that the determination of the surface energy or cleavage energy from slab energies is not necessarily straightforward. While we have shown that using a set of the largest slab energies to determine the appropriate value of the bulk energy converges more quickly and stably than other approaches, this does not give significantly more certain surface energy and cleavage energy results than other approaches when one considers results from different, equally valid treatments of the slab geometry.

We have also presented an analysis of the DOS of the $NaAlH_4$ surface. Such an analysis has not yet been presented in the literature. The surface DOS is important for understanding $NaAlH_4$ surface characteristics and thus can help elucidate hydrogen uptake and release mechanisms, one of the most pressing current issues in hydrogen storage materials research. Of particular interest would be how the surface states are affected by the addition of Ti; this is the subject of a forthcoming study.

A central theme of this paper has been the comparison of results calculated using different DFT methodologies. For the most common use of periodic DFT for complex metal hydride systems—the structure of bulk phases, there is generally a good level of agreement between the calculations performed in this work using DACAPO and VASP and previously published work. Pseudopotential calculations seem to be slightly less reliable for calculating lattice parameters (and thus bulk material densities). Expanding the application to surface properties and adding results calculated with ADF−BAND considerably reduces the level of agreement between different methodologies. This can have a serious impact on the confidence that one can have in surface properties calculated with any particular package. One is forced to consider whether the results obtained are a true reflection of the physics of the system under study or an artifact of the calculation method. In the calculations performed in this work, that was particularly the case for the DOS and the projection of the DOS onto atomic orbitals. Attribution of system states to H s states was particularly inconsistent. Some of the differences are explainable by subtle differences in the details of the calculation (such as projection onto hydrogenic orbitals versus projection onto multielectron orbital solutions for elemental atoms). That, however, does not alter the fact that any such subtle differences are rarely taken into consideration when interpreting calculated results. A further complicating factor when interpreting calculation results is that different DFT implementations present different capabilities. An example that arises in the present context is the capability of DACAPO to project DOSs onto "infinite extent" atomic orbitals rather than restrict the projection to orbitals truncated to a particular radius. Such a projection leads to very different local DOSs from those presented here, with greatly increased densities of Na s orbital states for the bulk and (001) and (100) surfaces, and (112) surface DOSs dominated by H states.

Unfortunately, direct comparisons between implementations such as these are rare. While we have identified some differences between the results produced by the three codes considered in this work, there is insufficient data to conclude which approaches are predicting more or less accurate surface properties.

Acknowledgment. This work was supported in part by a CW/NWO program grant and by the Norwegian Research Council.

References and Notes

(1) Schlapbach, L.; Züttel, A. *Nature* **2001**, *414*, 353.
(2) Bogdanović, B.; Schwickardi, M. *J. Alloys Compd.* **1997**, *253*, 1.
(3) Vajeeston, P.; Ravindran, P.; Vidya, R.; Fjellvåg, H.; Kjekshus, A. *Appl. Phys. Lett.* **2003**, *82*, 2257.
(4) Ke, X.; Tanaka, I. *Phys. Rev. B* **2005**, *71*, 024117.
(5) Opalka, S. M.; Anton, D. L. *J. Alloys Compd.* **2003**, *356*−*357*, 486.
(6) Íñiguez, J.; Yildirim, T.; Udovic, T. J.; Sulic, M.; Jensen, C. M. *Phys. Rev. B* **2004**, *70*, 060101(R).
(7) Peles, A.; Alford, J. A.; Ma, Z.; Yang, L.; Chou, M. Y. *Phys. Rev. B* **2004**, *70*, 165105.
(8) Aguayo, A.; Singh, D. J. *Phys. Rev. B* **2004**, *69*, 155103.
(9) Tsuda, M.; Dino, W. A.; Nakanishi, H.; Kasai, H. *J. Phys. Soc. Jpn.* **2004**, *73*, 2628.
(10) Løvvik, O. M.; Swang, O. *Europhys. Lett.* **2004**, *67*, 607.
(11) Løvvik, O. M. *Phys. Rev. B* **2005**, *71*, 144111.

(12) Łodziana, Z.; Vegge, T. *Phys. Rev. Lett.* **2004**, *93*, 145501.
(13) Frankcombe, T. J.; Kroes, G. J.; Züttel, A. *Chem. Phys. Lett.* **2005**, *405*, 73.
(14) Miwa, K.; Ohba, N.; Towata, S.; Nakamori, Y.; Orimo, S. *Phys. Rev. B* **2004**, *69*, 245120.
(15) Vajeeston, P.; Ravindran, P.; Kjekshus, A.; Fjellvåg, H. *J. Alloys Compd.* **2005**, *387*, 97.
(16) Arroyo y de Dompablo, M. E.; Ceder, G. *J. Alloys Compd.* **2004**, *364*, 6.
(17) Løvvik, O. M.; Opalka, S. M.; Brinks, H. W.; Hauback, B. C. *Phys. Rev. B* **2004**, *69*, 134117.
(18) Ge, Q. F. *J. Phys. Chem. A* **2004**, *108*, 8682.
(19) Chaudhuri, S.; Muckerman, J. T. *J. Phys. Chem. B* **2005**, *109*, 6952.
(20) Kohn, W.; Sham, L. J. *Phys. Rev.* **1965**, *140*, 1133.
(21) Hohenberg, P.; Kohn, W. *Phys. Rev. B* **1964**, *136*, 864.
(22) Parr, R. G.; Yang, W. *Density-Functional Theory of Atoms and Molecules*; Oxford University Press: New York, 1989.
(23) te Velde, G.; Baerends, E. J. *Phys. Rev. B* **1991**, *44*, 7888.
(24) Wiesenekker, G.; Baerends, E. J. *J. Phys.: Condens. Matter* **1991**, *3*, 6721.
(25) Hammer, B.; Hansen, L. B.; Nørskov, J. K. *Phys. Rev. B* **1999**, *59*, 7413.
(26) Bahn, S. R.; Jacobsen, K. W. *Comput. Sci. Eng.* **2002**, *4*, 56.
(27) Harrison, W. A. *Pseudopotentials in the Theory of Metals*; Benjamin: New York, 1967.
(28) Ihm, J.; Zunger, A.; Cohen, L. *J. Phys. C: Solid State Phys.* **1979**, *12*, 4409.
(29) Payne, M. C.; Teter, M. P.; Allan, D. C.; Arias, T. A.; Joannopoulos, J. D. *Rev. Mod. Phys.* **1992**, *64*, 1045.
(30) Vanderbilt, D. *Phys. Rev. B* **1990**, *41*, 7892.
(31) Kresse, G.; Furthmüller, J. *Comput. Mater. Sci.* **1996**, *6*, 15.
(32) Kresse, G.; Furthmüller, J. *Phys. Rev. B* **1996**, *54*, 11169.
(33) Blöchl, P. E. *Phys. Rev. B* **1994**, *50*, 17953.
(34) Kresse, G.; Joubert, J. *Phys. Rev. B* **1999**, *59*, 1758.
(35) Blöchl, P. E.; Först, C. J.; Schimpl, J. *Bull. Mater. Sci.* **2003**, *26*, 33.
(36) Slater, J. C. *Phys. Rev.* **1937**, *51*, 151.
(37) Frankcombe, T. J.; Kroes, G. J.; Choly, N. I.; Kaxiras, E. *J. Phys. Chem. B* **2005**, *109*, 16554.
(38) Kohler, B.; Wilke, S.; Scheffler, M.; Kouba, R.; Ambrosch-Draxl, C. *Comput. Phys. Commun.* **1996**, *94*, 31.
(39) Blaha, P.; Schwarz, K.; Madsen, G. K. H.; Kvasnicka, D.; Luitz, J. *WIEN2k, An Augmented Plane Wave + Local Orbitals Program for Calculating Crystal Properties*; Karlheinz Schwarz, Techn. Universität, Wien, Austria, 2001.
(40) Sjöstedt, E.; Nordström, L.; Singh, D. J. *Solid State Comm.* **2000**, *114*, 15.
(41) Madsen, G. K. H.; Blaha, P.; Schwarz, K.; Sjöstedt, E.; Nordström, L. *Phys. Rev. B* **2001**, *56*, 195134.
(42) Gonze, X.; Beuken, J.-M.; Caracas, R.; Detraux, F.; Fuchs, M.; Rignanese, G.-M.; Sindic, L.; Verstraete, M.; Zerah, G.; Jollet, F.; Torrent, M.; Roy, A.; Mikami, M.; Ghosez, P.; Raty, J.-Y.; Allan, D. C. *Comput. Mater. Sci.* **2002**, *25*, 478.
(43) Perdew, J. P.; Chevary, J. A.; Vosko, S. H.; Jackson, K. A.; Pederson, M. R.; Singh, D. J.; Fiolhais, C. *Phys. Rev. B* **1992**, *46*, 6671.
(44) Perdew, J. P.; Bourke, K.; Ernzerhof, M. *Phys. Rev. Lett.* **1996**, *77*, 3865.
(45) Perdew, J. P.; Bourke, K.; Ernzerhof, M. *Phys. Rev. Lett.* **1997**, *78*, 1396.
(46) Monkhorst, H. J.; Pack, J. D. *Phys. Rev. B* **1976**, *13*, 5188.
(47) Hauback, B. C.; Brinks, H. W.; Jensen, C. M.; Murphy, K.; Maeland, A. J. *J. Alloys Compd.* **2003**, *358*, 142.
(48) Løvvik, O. M. *J. Alloys Compd.* **2003**, *356*−*357*, 178.
(49) Fiorentini, V.; Methfessel, M. *J. Phys.: Condens. Matter* **1996**, *8*, 6525.
(50) Boettger, J. C.; Smith, J. R.; Birkenheuer, U.; Röcsh, N.; Trickey, S. B.; Sabin, J. R.; Apell, S. P. *J. Phys.: Condens. Matter* **1998**, *10*, 893.
(51) Boettger, J. C. *Phys. Rev. B* **1994**, *49*, 16798.
(52) Becke, A. D. *Phys. Rev. A* **1988**, *38*, 3098.
(53) Perdew, J. P. *Phys. Rev. B* **1986**, *33*, 8822.
(54) Hoffmann, R. *Solids and surfaces: A chemist's view of bonding in extended structures*; Wiley-VCH: New York, 1988.
(55) Majzoub, E.; McCarty, K. F.; Ozoliņš, V. *Phys. Rev. B* **2005**, *71*, 024118.
(56) Løvvik, O. M.; Swang, O. *J. Alloys Compd.* **2005**, *404*−*406*, 757.
(57) Løvvik, O. M.; Swang, O.; Opalka, S. M. *J. Mater. Res.* In press.